This is author version of article published as:
Perre, Patrick and Turner, Ian W. (2001) Determination of the Material Property Variations Across the Growth Ring of Softwood for Use in a Heterogeneous Drying Model - Part 1 Capillary Pressure, Tracheid Model and Absolute Permeability . Holzforschung 55(3):pp. 318-323.

Determination of the material property variations across the growth ring of softwood for use in a heterogeneous drying model

Part I – Capillary pressure, tracheid model and absolute permeability.

Patrick Perré
LERMAB (Laboratory of Wood Sciences) UMR INRA n° 1093
E.N.G.R.E.F., 14 rue Girardet, F-54042 Nancy Cedex, France

and

Ian Turner
School of Mathematical Sciences,
Queensland University of Technology,
GPO Box 2434, Brisbane, Q4001, Australia

Key Words: Capillary Pressure, Permeability, Tracheid model.

ABSTRACT

In this work, the extensive knowledge of wood gained at the *ENGREF* by using a combination of microscopic observation and experimental work is being used to postulate material property correlations for a macroscopic heterogeneous "*Cerne*" growth ring model of softwood. Mathematical tools such as image analysis and homogenisation are used to develop models that capture the effect of the density variation within the wood sample of important macroscopic physical parameters. This first part is devoted to mass transfer in wood due to Darcy's law. Capillary pressure correlations as a function of local density are deduced from image analysis. Thereafter, a tracheid model is proposed for softwood. Its shape evolves from earlywood to latewood according to anatomical observations. Liquid and gaseous permeability values are calculated from this model according to Poiseuille's flow within cells and assuming a linear flow-pressure loss relationship through the pits.

1. INTRODUCTION

Tracheids account for 95% of the mass of softwoods (Siau 1984). Tracheids are formed in the radial direction by the division of the same initial cell in the cambium. For this reason, the cell walls are aligned in this direction. In the tangential direction,

the cells are randomly arranged. From earlywood to latewood, the tangential diameter is almost constant, but the radial diameter decreases and the cell wall thickness increases (Wilson and White 1984). Consequently, the density varies by a factor ranging between three and four for wood elaborated in spring and wood elaborated in late summer. Density variation within the growth ring usually is measured by radiography analysis (Polge 1966). However, Perré (1997) has shown that image analysis also can be used to obtain the local density variation on a microtome section. As a result of this density variation, almost all of the physical parameters are affected strongly by the position within the annual ring. The object of this two part paper is to develop correlations that capture the effect of density on each physical parameter required for use in a computational model known as *TransPore* (Perré and Turner, 1999a-b) that simulates the wood drying process. The required correlations have been derived using literature data, image analysis measurements and physical considerations that take the wood anatomy into consideration. The main purpose of the work is to prepare a set of expressions that will allow the drying simulation of a section of softwood to be computed when taking into account the alternation of earlywood and latewood. The presentation of this heterogeneous drying model and the presentation of the simulation results are the objective of a future paper. In Part I of this work, the capillary pressure and absolute permeability correlations will be derived and in Part II, the bound liquid diffusivity and thermal conductivity correlations will be discussed.

2. DERIVATION OF THE MACROSCOPIC WOOD PROPERTIES

2.1 Basic variable definitions used throughout this section

The following variables will be referred to and used often throughout this section:

f ° Porosity

r_s ° Density of the cell-wall substance (r_s = 1530 kg m^{-3})

r_0 ° Specific wood density (oven dry mass/ green volume)

ρ_l ≡ Water density ($\rho_l = 1000$ kg m^{-3})

X ≡ Moisture content (kg water / kg of dry wood)

X_l ≡ Free water moisture content

X_b ≡ Bound water moisture content

X_{FSP} ≡ Fibre Saturation Point

T ≡ Temperature ^{o}C

Because wood is highly hygroscopic, bound water has to be separated from free water to give the expression:

$$X = X_b + X_l \qquad [1]$$

where $X_b = \min(X_{fsp}, X)$

and $X_{fsp} = 0.325 - 0.001T$ (at full saturation, $X_{sat} = X_{fsp} + X_{l\max}$)

The saturation variable is calculated according to the free water content only:

$$S_l = \frac{X_l}{X_{l\max}} \qquad [2]$$

Assuming that the volume of the pores is constant and that the density of bound water and free water are equal, the following expression has been derived for the volume fraction of the solid phase:

$$e_s = \frac{1 + \frac{r_s X_b}{r_l}}{\left(\frac{r_s}{r_0} + \frac{r_s}{r_l}(X_b - X_{fsp})\right)} \qquad [3]$$

The porosity is defined as $\phi = (1 - \varepsilon_s)$ and the volume fractions of the liquid and gaseous phases are given respectively by

$$\varepsilon_l = \phi S_l \text{ and } \varepsilon_g = \phi (1 - S_l) \qquad [4]$$

2.2 Capillary Pressure

Due to the large density variation that can be observed in softwood within the annual ring, it can be concluded that the pores in the latewood component of the annual ring are smaller than in the earlywood component. Consequently, stronger capillary forces become evident in latewood. The partition of pore size can be obtained from image analysis (Perré, 1996). These results are in good agreement with results calculated from mercury porosimetry on thin cross sections of wood (Trénard 1980). Figure 1 depicts a typical cross-section of Spruce observed using an optical microscope, as well as the pore size distribution, as determined by image processing on three different zones. The following mathematical expression has been elaborated from the averaged pore size partition determined for the same local density on several annual rings:

$$P_c(S_l, T, r) = s(T) \left\{ \frac{3150}{S_l + 1 \times 10^{-4}} - \frac{1047 + 3.368 r_0}{1.02 - S_l} + 149.8 r_0 (1 - S_l) + 52350 + 168.4 r_0 - \frac{3150}{1 + 1 \times 10^{-4}} \right\} \qquad [5]$$

This expression assumes that the liquid partition minimizes the energy of the surface tension. In equation [5] P_c is in Pascal (Pa) and $s(T) = (77.5 - 0.185T) \times 10^{-3}\ N\,m^{-1}$ represents the surface tension of water. The variation of capillary pressure plotted against liquid saturation for various densities is depicted in Figure 2 for a temperature of $30^o C$. The curves show that as the wood density increases from $200\,\mathrm{kg\,m^{-3}}$ up to $1000\,\mathrm{kg\,m^{-3}}$, the capillary pressure increases in magnitude, due to the reduction in averaged pore diameter.

A different view of these variations is exhibited in Figure 3, where in this instance capillary pressure has been plotted against liquid moisture content X_l. This choice of

this variable allows the maximum moisture content to be exhibited as a function of density. It is clear from the curves that much more water can be retained in the earlywood regions as opposed to the latewood regions of the annual ring. Indeed, we have to keep in mind that moisture content is the ratio between the mass of water and the mass of solid - in earlywood the pore volume is high and the solid density is low. Consequently, the maximum moisture content is around 500 % against 60% in latewood. Figure 3 provides the perfect mechanism to understand the distribution of liquid versus the capillary pressure curve:

- Low values of capillary pressure provide a moisture content higher in earlywood than in late wood.
- High values of capillary pressure provide a moisture content higher in latewood than in earlywood, because of the smaller size of the pores in this part of the annual ring.

2.3 Tracheid model

As explained in the introduction, the average tracheid shape evolves significantly between earlywood and latewood. In the following sections of this paper a description of this evolution is required. Recall that the tracheids are created in the radial direction by the division of the same initial cell in the cambium. Due to this alignment, the tangential dimension (a_T) is almost constant. According to microscopic observations, the value $a_T = 50\,\mu m$ was admitted here. The tracheid length (a_L) also is required to evaluate the longitudinal permeability. Softwoods are well known to have long fibers having length somewhere between 2 to 4 mm (Wilson and White 1984). Nevertheless, due to overlapping, the mean distance between two adjacent tracheids is less. The value used here for the longitudinal direction is $a_L = 1.5\,mm$.

The radial dimension (a_R) as well as the double cell wall thickness change with position within the annual growth ring. It is assumed that these quantities vary with density only across the annual ring. This variation is postulated to be linear, $a_R(\rho) = c_1 + c_2\rho$. The constants c_1 and c_2 are determined by assuming that $a_R(200) = a_T$ and $a_R(1000) = 20\,\mu m$ to obtain the expression for the radial dimension of the tracheid as

$$a_R(\rho) = 0.575 \times 10^{-4} - 0.375 \times 10^{-7}\rho \quad (m) \ . \qquad [6]$$

Since the walls of the earlywood tracheids are thinner than the walls of a latewood tracheid, a function, shown in Figure 4 as $t_v(\rho)$, is introduced into the virtual tracheid representation in order to capture this wall thickness variation with density.

It follows from its very definition that the porosity of the virtual tracheid is obtained by evaluating the ratio of void volume to the total volume:

$$\phi \equiv \frac{\text{Void Volume}}{\text{Total Volume}} = \frac{\left(a_R(\rho) - 2t_v(\rho)\right)\left(a_T(\rho) - 2t_v(\rho)\right)}{a_R(\rho)a_T} \ . \qquad [7]$$

Recalling that the porosity is defined also by the expression $\phi = 1 - \varepsilon_s(\rho)$ it becomes possible to write an equation that enables $t_v(\rho)$ to be determined for a given density:

$$1 - \varepsilon_s(\rho) - \frac{\left[a_R(\rho) - 2t_v(\rho)\right]\left[a_T(\rho) - 2t_v(\rho)\right]}{a_R(\rho)a_T} = 0 \quad . \qquad [8]$$

Clearly equation [8] indicates that there are two possible roots for a given value of ρ. However, only one of these roots provides the correct physical behaviour over the closed interval $\rho \in [200,1000]$ namely, $t_v(\rho)$ increasing with increasing density. After solving [8] for this root to obtain a data set of the form $\{\rho_1, t_{v1}, \rho_2, t_{v2}, \rho_3, t_{v3}, \ldots, \rho_n, t_{vn}\}$ for $\rho_n = 200 + n$, $n = 0,5,10,\ldots,800$, the following cubic polynomial is fitted through the data in the least squares sense:

$$t_v(\rho) = .53733443 \times 10^{-6} + .66577831 \times 10^{-8}\rho + .10275104 \times 10^{-10}\rho^2 - .82567033 \times 10^{-14}\rho^3 \quad (m) \quad . \qquad [9]$$

The use of this polynomial expression enables an efficient evaluation of cell wall thickness for $\rho \in [200,1000]$ (Figure 5).

2.4 Absolute Permeabilities for the Liquid and Gaseous phases

This section is devoted to determining the density variation across the growth ring of the absolute permeabilities for the liquid and gaseous phases. The evaluation of these parameters uses the tracheid model defined section 2.3. The fluid flow into softwood uses tracheid lumina and passes from one tracheid to the other through bordered pits. The resistance to the fluid flow in the lumina can be calculated according to classical equations of steady-state fluid flow in ducts. This resistance will be neglected in the transverse directions (R and T). The resistance to fluid flow through the pits is calculated according to singular pressure drops and is described in the permeability models presented throughout this section via the parameter $\alpha(\rho)$. This parameter effectively represents the pressure drop times the fluid viscosity divided by the corresponding fluid flux. It has been assumed to depend upon the tracheid wall thickness according to the following linear relation:

$$\alpha(\rho) = c_3 t_v(\rho) + c_4 \quad . \qquad [10]$$

This relation accounts, in a simplistic way, for both the singular pressure drop due to constriction (the resistance does not tend towards zero with the cell wall thickness) and to the evolution of pit shape between earlywood and latewood (longer pathway and smaller diameter). It is assumed that the number of pits available for radial (n_R) and tangential (n_T) flow is proportional to the corresponding lumen area dimensions. Referring to Figure 4, the relevant expressions for the number of pits can be written in a mathematical context as follows:

$$n_R = \gamma\left[a_T - 2t_v(\rho)\right], \; n_T = \gamma\left[a_R - 2t_v(\rho)\right] \qquad [11]$$

The number of pits available in the longitudinal direction of the tracheid is taken simply as the sum $n_L = n_R + n_T$. In this work, the value used for the proportionality constant is $\gamma = \frac{25}{a_T}$, which gives a reasonable total number of pits equal to a 50 per overlapping zone in earlywood.

The next stage in the derivation of the permeability correlations is to determine the velocity distribution for steady unidirectional flow of a uniform incompressible viscous fluid in a tube of rectangular cross section whose sides are at $y = \mp b, z = \mp c,\ c > b$. In this case, it becomes necessary to solve the following Poisson equation for $u(y,z)$ (Batchelor, 1970):

$$\frac{\partial^2 u}{\partial y^2} + \frac{\partial^2 u}{\partial z^2} = -\frac{G}{\mu} \qquad [12]$$

subject to the boundary conditions

$$\begin{aligned} u(-b,z) &= u(b,z) = 0 \\ u(y,-c) &= u(y,c) = 0 \end{aligned} \qquad [13]$$

In equation [12], -G is a fixed constant pressure gradient and μ is the dynamic viscosity.

The solution to the system [12-13] can be derived as

$$u(y,z) = \frac{G}{2\mu}\left(b^2 - y^2 + \sum_{n\ \text{odd}} A_n \cosh\left(\frac{n\pi z}{2b}\right)\cos\left(\frac{n\pi y}{2b}\right)\right), \qquad [14]$$

where the coefficients are given by

$$A_n = \frac{G}{2\mu b \cosh\left(\frac{n\pi c}{2b}\right)} \int_{-b}^{b} \left(c^2 - b^2\right)\cos\left(\frac{n\pi y}{2b}\right) dy \ . \qquad [15]$$

The volume flux past any section of the tube is given as

$$Q = \int_{-b}^{b}\int_{-c}^{c} u(y,z)\,dy\,dz \ . \qquad [16]$$

Referring again to Figure 4, it is possible to determine the volume flow past any section of the virtual tracheid lumen by taking $b = \frac{a_R(\rho)}{2} - t_v(\rho)$, $c = \frac{a_T}{2} - t_v(\rho)$ and note that the first *fifteen terms* in the series of equation [14] have been used for the computations.

The parameter $\beta(\rho) = \frac{\mu Q}{G}$ then is fitted using a data set of the form $\{\rho_1, \beta_1), (\rho_2, \beta_2), (\rho_3, \beta_3), \ldots, (\rho_n, \beta_n)\}$ for $\rho_n = 200 + 50n$, $n = 0,\ldots,16$, to obtain the following quartic least squares polynomial:

$$\begin{aligned}\beta(\rho) = {} & 0.27514032 \times 10^{-18} - 0.71386999 \times 10^{-21}\rho + 0.46368212 \times 10^{-24}\rho^2 \\ & + 0.12115020 \times 10^{-27}\rho^3 - 0.14614421 \times 10^{-30}\rho^4\end{aligned} \qquad [17]$$

Although expression [17] is only an approximation of that obtained using the complete calculation, it enables a fast and reasonably accurate evaluation of $\beta(\rho)$ across the interval $\rho \in [200,1000]$.

2.4.1 Liquid Permeability

The liquid permeability correlations are given for the radial, tangential and longitudinal directions of the wood as:

$$\begin{aligned} k_R(r) &= \frac{n_R(r)a_R(r)}{2a_T a_L a(r)}, \\ k_T(r) &= \frac{n_T(r)a_T}{2a_R(r)a_L a(r)}, \\ k_L(r) &= \frac{a_L}{a_T a_R(r)\left(\frac{a(r)}{n_L(r)} + \frac{a_L}{b(r)}\right)} \end{aligned} \qquad [18]$$

The justification for the use of [17] can be realised easily now when one imagines the amount of additional computation that would be necessary if the complete analytical expression were used in determining a value for the longitudinal permeability for any $\rho \in [200,1000]$.

The variation of liquid permeability plotted versus density on a $\log_{10}$ scale is given in Figure 6 for the radial, tangential and longitudinal directions of wood. In equation [10] the coefficients c_3 and c_4 are chosen to calibrate the permeability relations to lie within the range of experimental measurement. In this work the values $c_3 = 1.8 \times 10^{24}$ and $c_4 = 2 \times 10^{-6}$ provided such a calibration. Using these values, the difference between earlywood and latewood is approximately a ratio of ten, which is in agreement with the values proposed by Bolton and Petty (1978).

2.4.2 Gas Permeability

The primary contrast between the gaseous and liquid phase permeability concerns the aspiration of the pits. Indeed, gas flow can occur in a pit only after free water has been removed from both sides of this pit, implying that the liquid-gas meniscus has passed through this pit, with possible torus aspiration (Comstock and Cote 1968, Wilson and White 1984). However, due to the change in pit geometry, aspiration is by far less likely to appear in latewood than in earlywood. Bolton and Petty (1978) estimated that the pressures required for aspirating the torus were 5.6×10^5 Pa for earlywood and

6.8×10^5 Pa for latewood. According to the surface tension of water at 20°C, the corresponding pore radii are respectively equal to 0.21 µm and 0.018 µm. With regards to the margo anatomy, it becomes evident that almost all pits should be aspirated in earlywood and none in latewood. In this case, equation [11] should involve an "aspiration" function that depends on the wall thickness:

$$n_R = A_s(t_v)\gamma\left(d_T - 2t_v(\rho)\right) \quad n_T = A_s(t_v)\gamma\left(d_R - 2t_v(\rho)\right). \qquad [19]$$

The particular aspiration functional form $A_s(t_v)$ used in this work has an exponential shape that results in 5% of non-aspirated pits in earlywood up to 100% in latewood, Figure 7. The gaseous phase absolute permeability correlations for each of the radial, tangential and longitudinal directions are computed using equation [18] with the new pit relations [19]. Their variation with density has been exhibited in Figure 8 using a $\log_{10}$ scale.

3. CONCLUSIONS

In this work, the use of image analysis and a simple tracheid model has enabled correlations to be proposed for calculating the effect of density variation on the physical transport properties : capillary pressure and absolute permeability. The models presented throughout Part I remain closely tied to the physics of wood and have been based on classical wood science arguments. The concept of the virtual tracheid model can now be used in Part II of this work to develop, with the aid of homogenisation arguments, density dependent correlations for bound liquid diffusivity and thermal conductivity.

4. ACKNOWLEDGEMENT

One of the Authors, Ian Turner, would like to thank the French organisation INRA for funding his visit to the ENGREF/INRA laboratory to enable this work to be realised. The travel assistance offered under the Personal Development Program at the QUT should be acknowledged also.

5. REFERENCES

Batchelor G.K. "An introduction to fluid dynamics" Cambridge University Press, 1970.

Bolton A.J. and Petty J.A. "A model describing axial flow of liquids through conifer wood" Wood Sci. Technol. 12: 38-48 (1978A).

Bolton A.J. and Petty J.A. "The relationship between the axial permeability of wood to dry air and to a non-polar solvent" Wood Sci. Technol. 12: p.111-126 (1978B).

Comstock G.L. and Cote W.A."Factors affecting permeability and pits aspiration in coniferous sapwood" Wood Sci. Techn.,Vol.2, 279-291 (1968).

Perré P. "Image Analysis, Homogenization, Numerical Simulation and Experiment as Complementary Tools to Enlighten the Relationship between Wood Anatomy and Drying Behavior" Drying Technology Journal, 15(9), 2211-2238 (1997).

Perré P. and Turner I. " TransPore: A Generic Heat and Mass Transfer Computational Model for Understanding and Visualising The Drying Of Porous Media" Invited paper, Drying Technology Journal, 17(7), 1273-1289 (1999a).

Perré P. and Turner I. "A 3D version of TransPore : A Comprehensive Heat and Mass Transfer Computational Model for Simulating the Drying of Porous Media" Int. J. Heat Mass Transfer, 42(24), 4501-4521 (1999b).

Polge H. “Etablissement des courbes de variations de la densité du bois par exploration densitometrique de radiographies d’échantillons prélevés à la tarière sur les arbres vivants. Application dans les domaines technologiques et physiologiques: Utilisation des spectres de diffraction des rayons X pour les études de la qualité du bois." – PhD thesis, Faculté des sciences de Nancy 1 (1966).

Siau, J.F., "Transport Processes in Wood" Springer-Verlag (1984).

Trenard Y. "Comparaison et interprétation de courbes obtenues par porosimétrie au mercure sur divers essences de bois" Holzforschung Bd. 34 H.4 (1980).

Wilson K. and White D.J.B. "The anatomy of wood : its density and variability" Storbart & Son Ltd, London (1984).

FIGURES CAPTIONS

Figure 1 : Cross section of Spruce that depicts the continuous structure variation from earlywood to latewood (picture J.C. Mosnier, ENGREF). The corresponding pore size partition as determined by image processing is depicted for three different zones (earlywood, intermediate wood and latewood).

Figure 2 : Capillary Pressure versus Liquid Saturation for various Wood Densities

Figure 3 : Capillary Pressure versus Liquid Moisture Content for various Densities

Figure 4 : The Virtual Tracheid Model

Figure 5 : Wall Thickness and Radial Dimension variation with Density for the Virtual Tracheid

Figure 6 : Variation of Liquid Permeability with Density in the Radial, Tangential and Longitudinal Directions of Wood

Figure 7 : Variation of Aspiration Function with Tracheid Wall Thickness

Figure 8 : Variation of Gas Permeability with Density in the Radial, Tangential and Longitudinal Directions of Wood

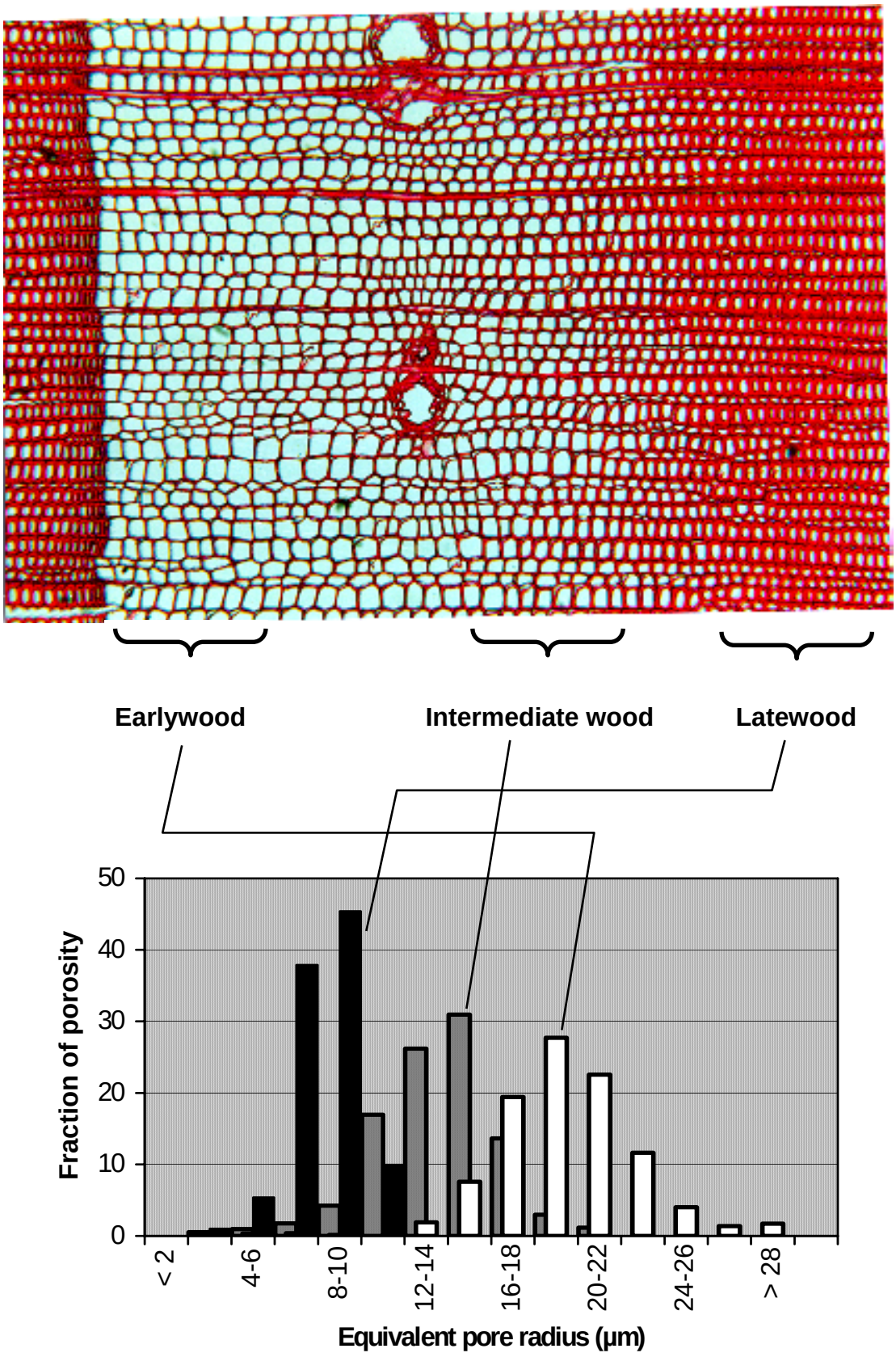

Figure 1 : Cross section of Spruce that depicts the continuous structure variation from earlywood to latewood (picture J.C. Mosnier, ENGREF). The corresponding pore size partition as determined by image processing is depicted for three different zones (earlywood, intermediate wood and latewood).

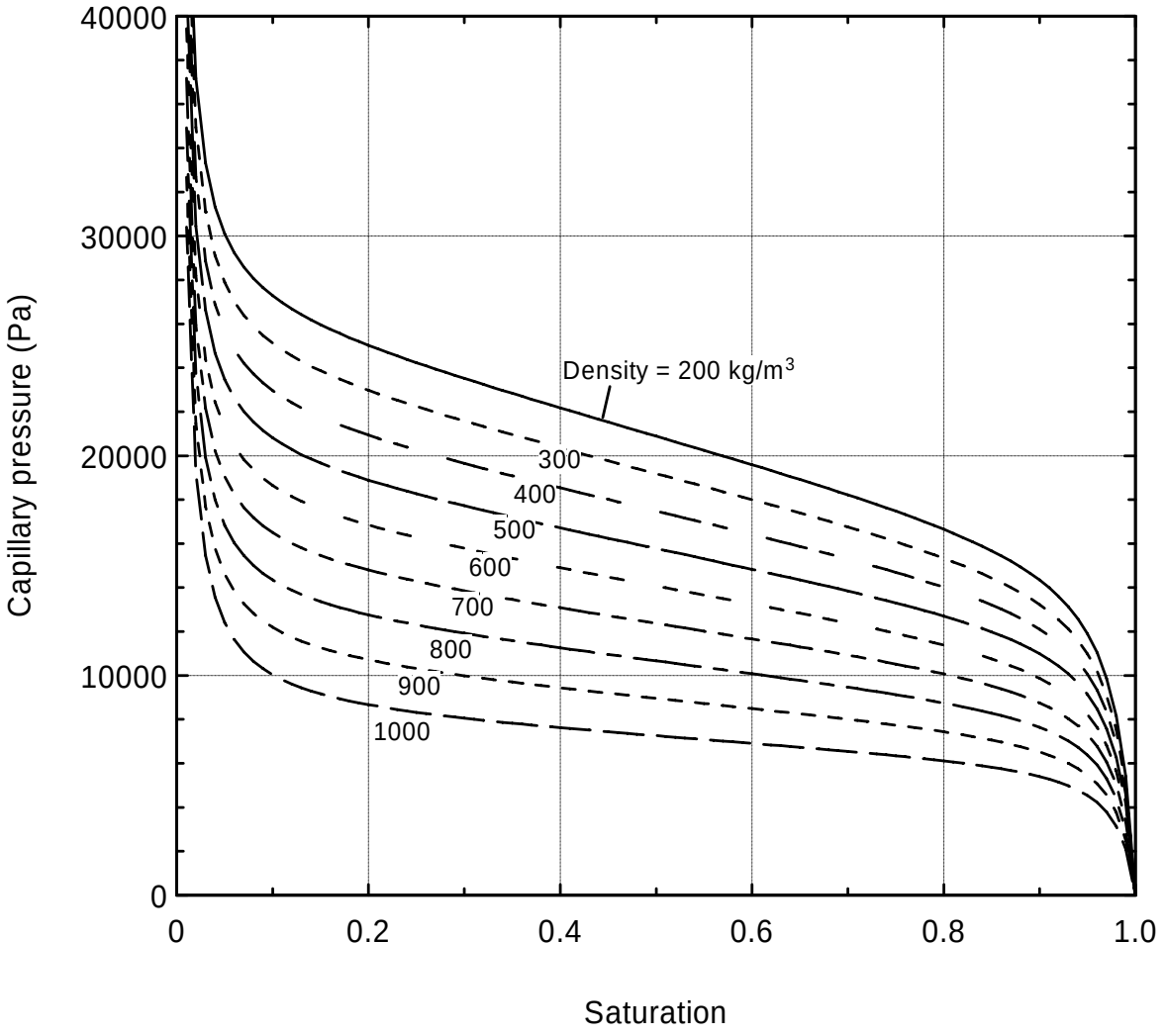

Figure 2 : Capillary Pressure versus Liquid Saturation for various Wood Densities

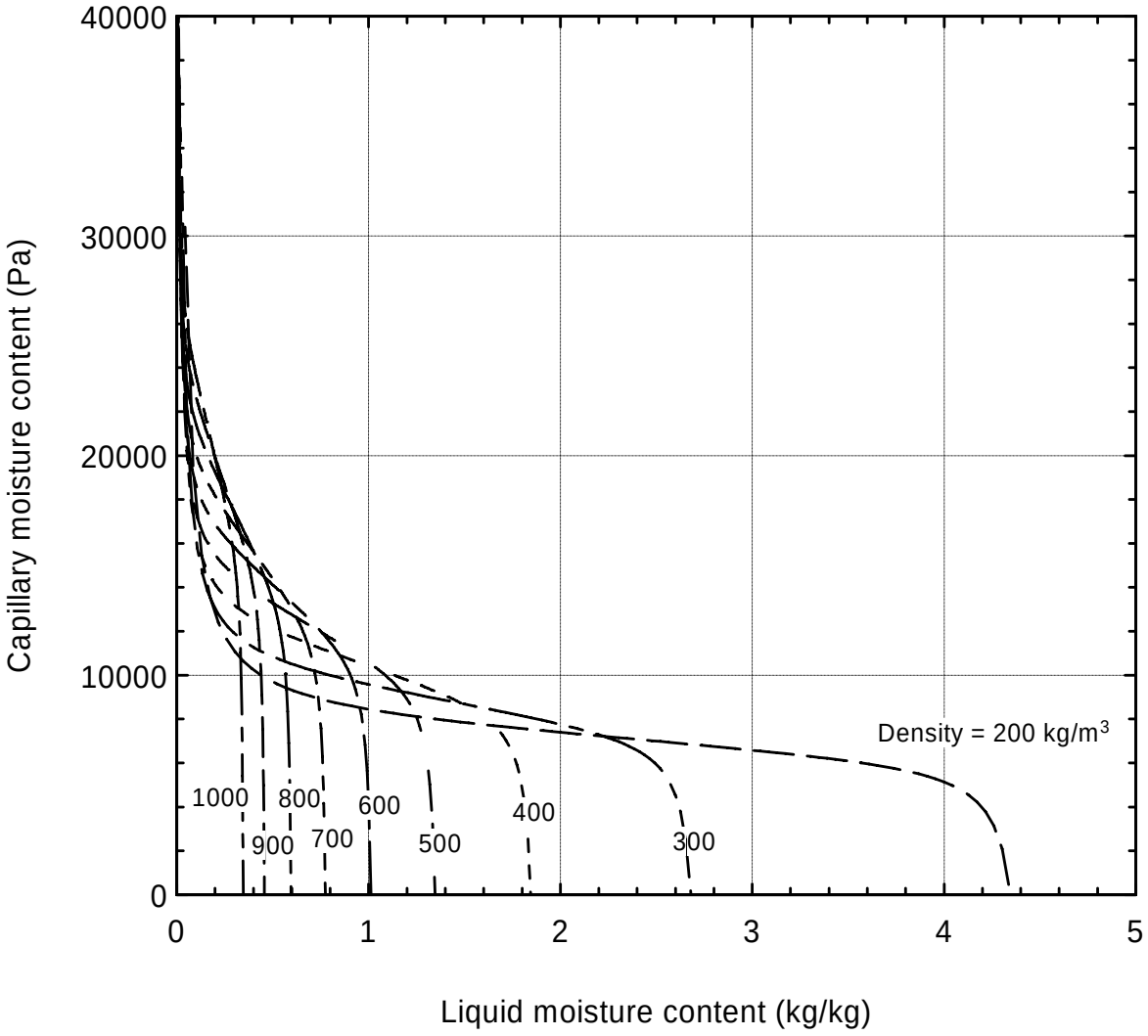

Figure 3 : Capillary Pressure versus Liquid Moisture Content for various Densities

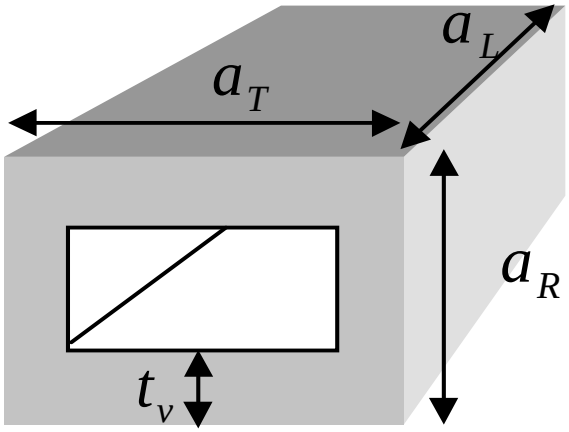

Figure 4 : The Virtual Tracheid Model

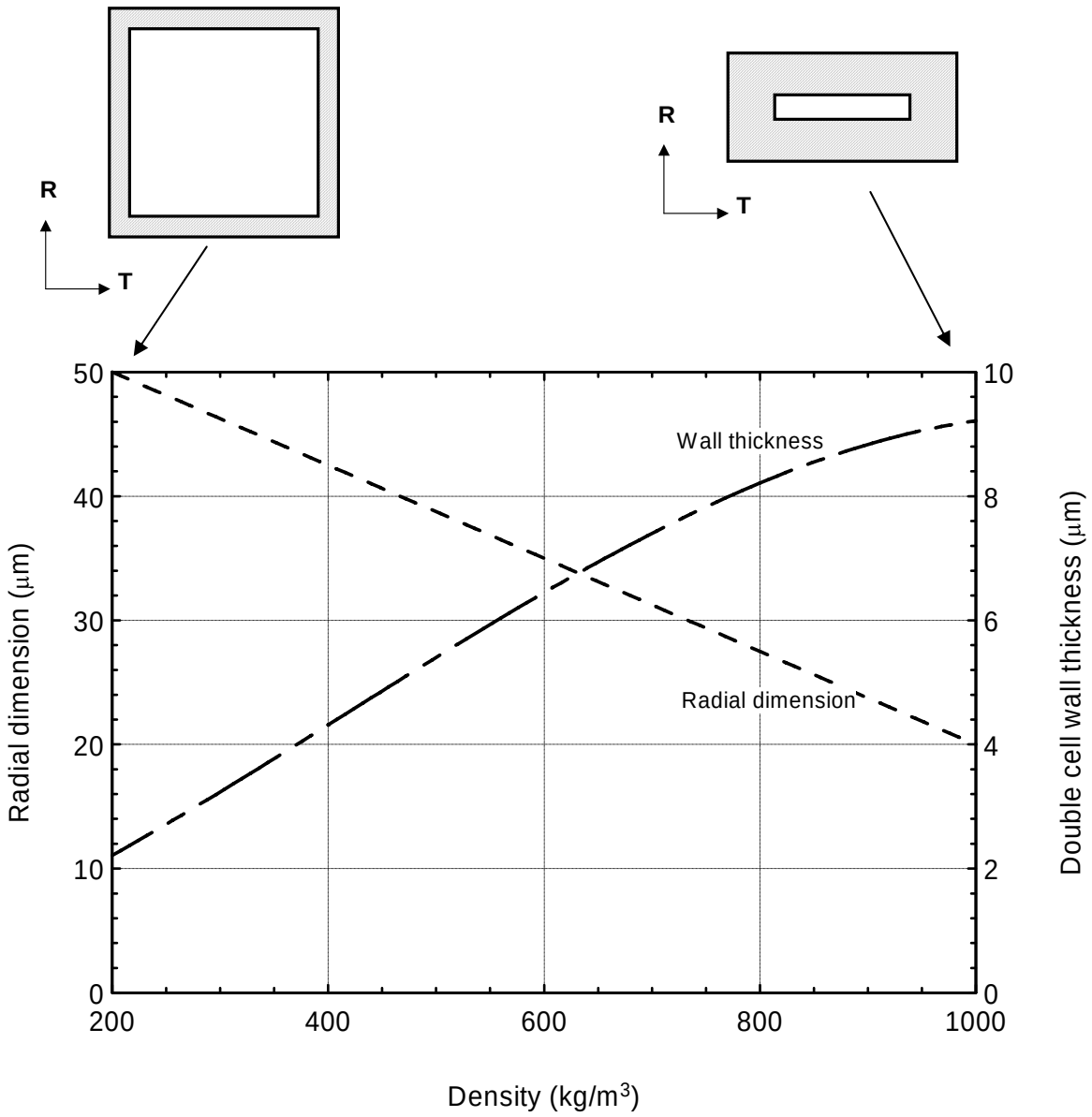

Figure 5 : Wall Thickness and Radial Dimension variation with Density for the Virtual Tracheid

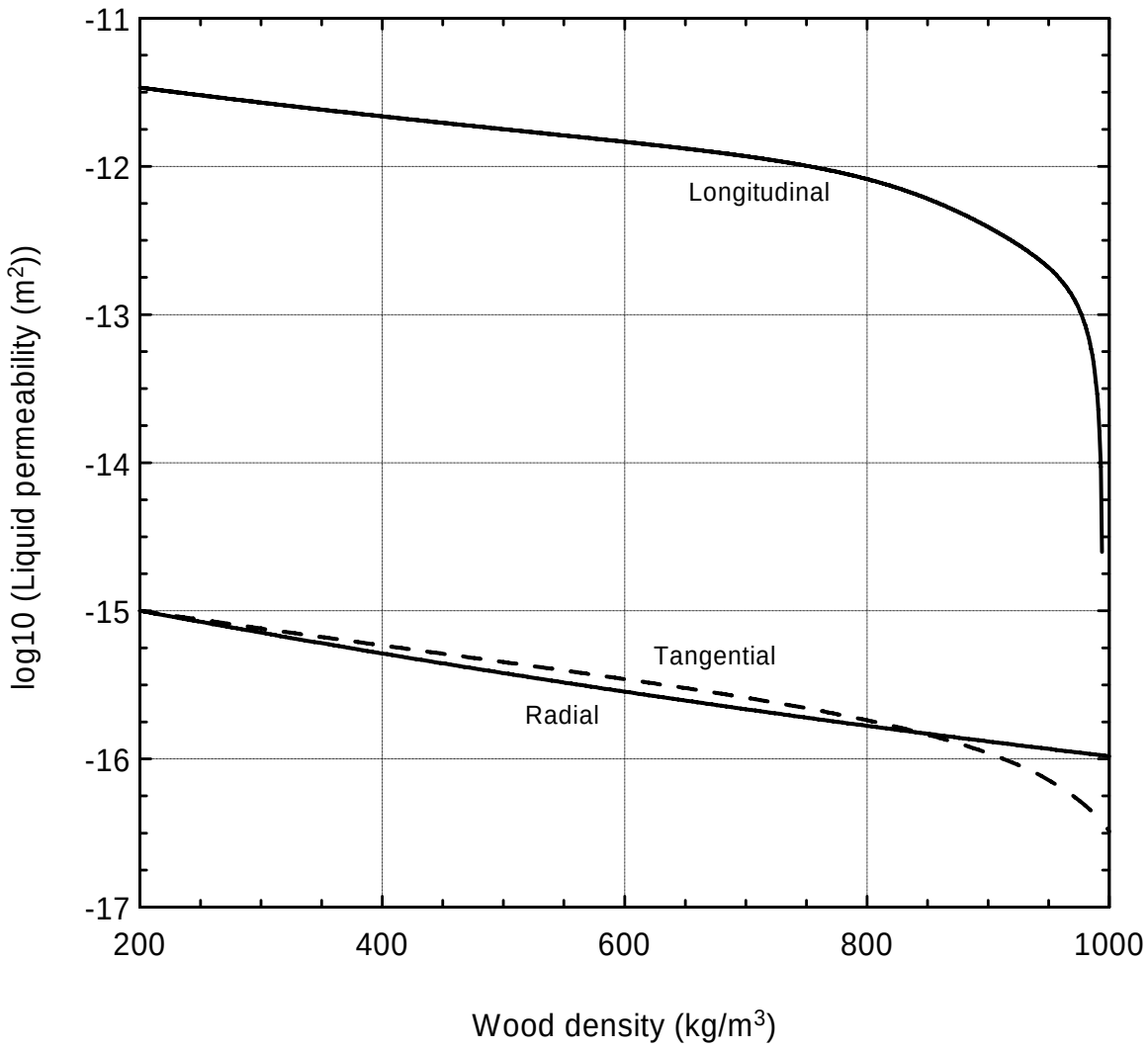

Figure 6 : Variation of Liquid Permeability with Density in the Radial, Tangential and Longitudinal Directions of Wood

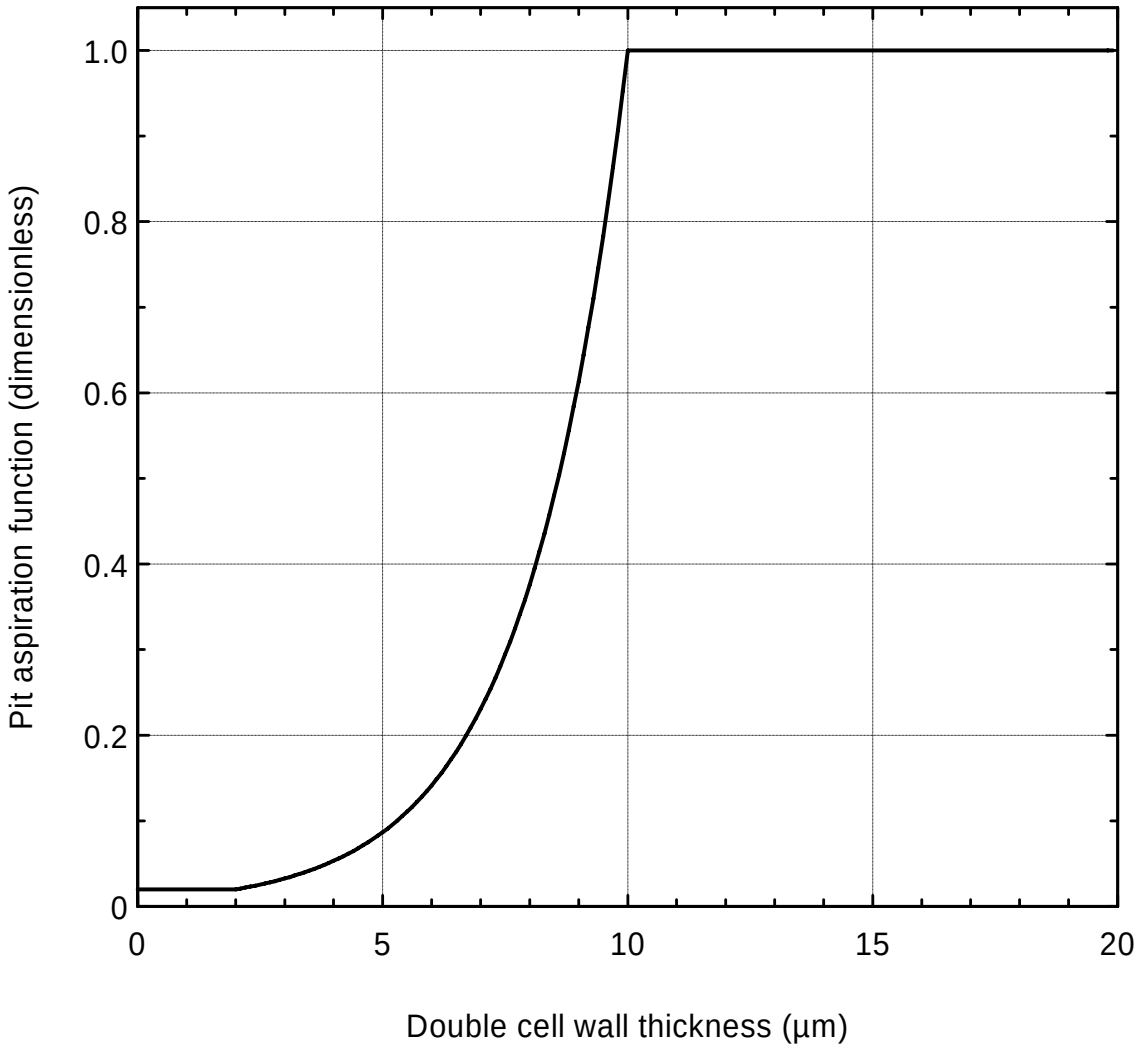

Figure 7 : Variation of Aspiration Function with Tracheid Wall Thickness

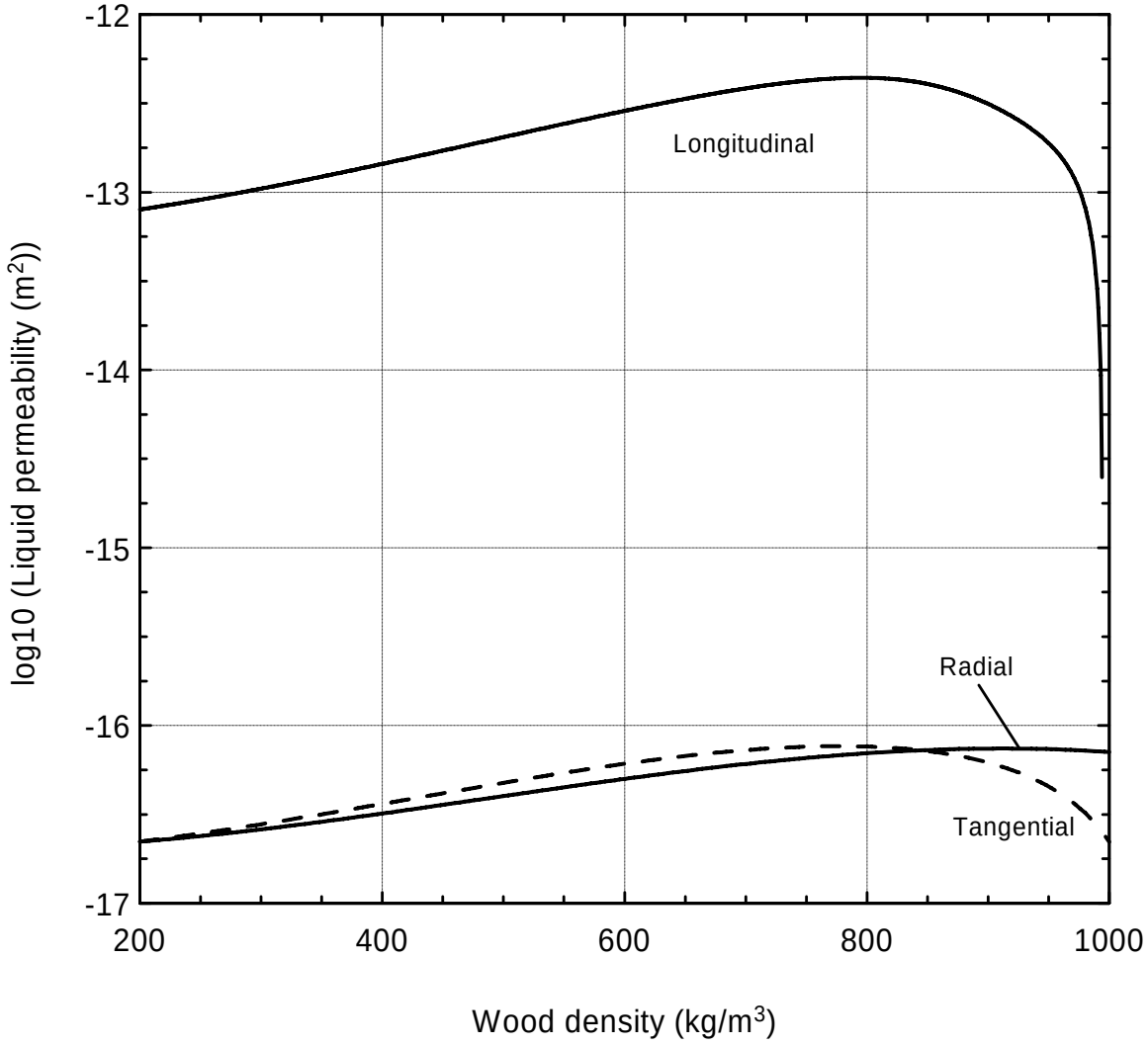

Figure 8 : Variation of Gas Permeability with Density in the Radial, Tangential and Longitudinal Directions of Wood